Letter

Direct Measurement of Ballistic and Diffusive Electron Transport in Gold

Pravin Karna, Md Shafkat Bin Hoque, Sandip Thakur, Patrick E. Hopkins, and Ashutosh Giri*

Cite This: *Nano Lett.* 2023, 23, 491−496

Read Online

ACCESS | 📊 Metrics & More | 📰 Article Recommendations | 🗎 Supporting Information

ABSTRACT: We experimentally show that the ballistic length of hot electrons in laser-heated gold films can exceed ∼150 nm, which is ∼50% greater than the previously reported value of 100 nm inferred from pump−probe experiments. We also find that the mean free path of electrons at the peak temperature following interband excitation can reach upward of ∼45 nm, which is higher than the average value of 30 nm predicted from our parameter-free density functional perturbation theory. Our first-principles calculations of electron−phonon coupling reveal that the increase in the mean free path due to interband excitation is a consequence of drastically reduced electron−phonon coupling from lattice stiffening, thus providing the microscopic understanding of our experimental findings.

Hot electrons travel further

KEYWORDS: electron−phonon coupling, plasmonics, ballistic electrons, density functional perturbation theory
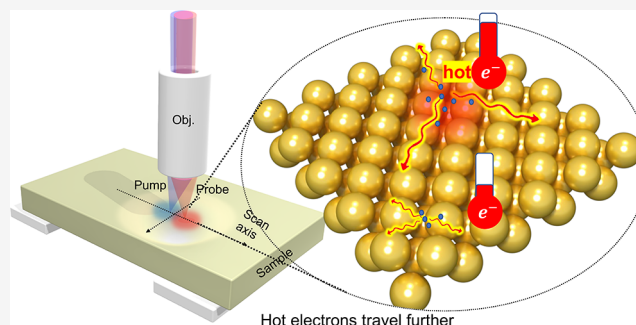
The fundamental electronic transport processes in metals have been of foundational interest to a wide array of physics, chemistry, and engineering disciplines since Drude's work describing the scattering processes of a free electron gas.[1] A key process in Drude's theory, and subsequent more robust theories of electronic transport in metals,[2,3] is the electron−phonon scattering rate, which is the critical process that underpins a wide array of optical, electrical, magnetic, and thermal properties in materials processing,[4−6] plasmonics,[7−9] nanophotonics,[10] photovoltaics,[8,11,12] photocatalysis, and non-linear optics.[13−16] For example, in plasmonic devices, the nonradiative plasmon decay involving the generation of hot carriers in a metallic layer, which can ballistically transfer their energies to underlying semiconductor layers without interacting with the relatively "colder" lattice,[9,17] can be used for applications in solar energy harvesting. Likewise, the fundamental understanding of electron−phonon scattering processes is also of significance to various phenomena in condensed matter physics such as spin caloritronics,[18,19] superconductivity,[20] and energy transport.[21] Therefore, considerable prior work has been devoted to understanding the coupling within and between the fundamental energy carriers in metals.

The dynamics of electron−phonon coupling and the relaxation of free electron gas have been routinely studied via ultrafast pump−probe experiments.[7,22−28] This is owing to the substantially lower heat capacity of the electronic subsystem with respect to that of the lattice, which allows the monitoring of the selective perturbation of electron gas and the concomitant energy relaxation processes following laser excitation. In gold, for example, the excited electrons do not achieve a Fermi−Dirac distribution at temporal regimes of <600 fs where these nonequilibrium carriers traverse ballistically with velocities close to the Fermi velocity.[22,29−31] For this regime, a mean free path of 100 nm has been inferred through various pump−probe experiments on gold films with varying thicknesses.[22,29,31] Several works have also alluded to the possibility of the ballistic range of electrons to be in the 100 to 200 nm range.[32,33] For example, by modeling the ultrafast laser melting threshold in gold, Chowdhury et al. have shown that the melting threshold behavior can only be explained by including ballistic mean free paths of ∼200 nm in their model.[33] However, a direct measurement of the ballistic length has remained elusive thus far. Once equilibration is reached among the hot carriers through carrier−carrier scattering,[30] hot electron diffusion through electron−phonon coupling subsequently cools and thermalizes these hot carriers with the lattice vibrations within a few picoseconds.[23,34,35] This regime of diffusive electron dynamics has been shown to be well described by various rate-relaxation models such as the two-temperature model when compared to pump−probe measurements.[25,36−38] More rigorous modeling based on
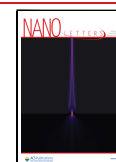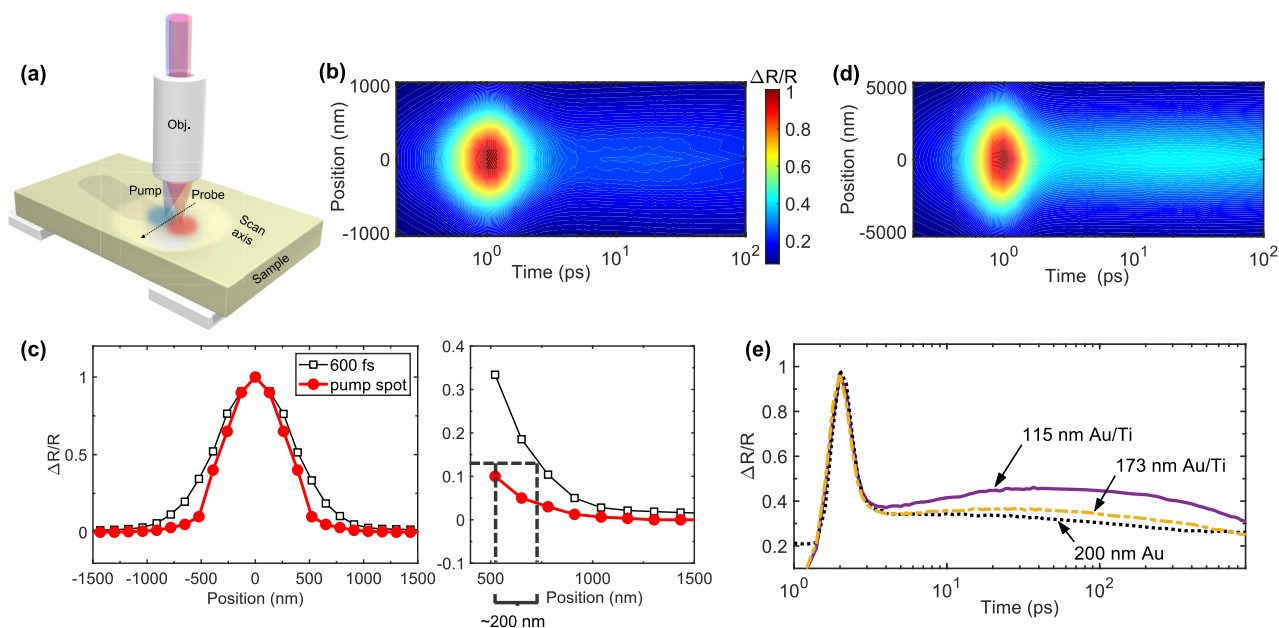
Figure 1. (a) Schematic of the ultrafast super-resolution thermoreflectance experiment showing the unique capability of moving a diffraction limited pump along a scan axis relative to a stationary probe that interrogates the surface response induced by the offset pump. (b) Characteristic contour profile showing the spatiotemporal response with nanometric precision of a 200 nm thick gold film. (c) Monitoring the Gaussian profile of the reflected probe at time delays of <600 fs provides insight into the dynamics of nonthermal electrons in the gold film that ballistically traverse with velocities close to the Fermi velocity. Compared to our laser spot size (at the location where the intensity has decayed by $1/e^2$), we find signals in excess of ~200 nm. (d) Spatiotemporal response of a 150 nm thick Au film with a 2 nm Ti layer in between the film and the substrate. (e) Immediately after laser irradiation of the Au/Ti structure, ballistic electrons from the gold deposit their energy at the Ti layer due to the relatively higher electron−phonon coupling factor. A "rerise" in the reflected probe signal in the 5 to 50 ps time regime shows the surface reflectivity increase of the gold film through heat conduction originating from the Ti layer.

parameter-free *ab initio* calculations that directly solve Fermi's golden rule have predicted mean free paths in the range of 20 to 30 nm for electrons around the Fermi energy of gold.[39,40] Unresolved, however, is the direct measurement of the characteristic length scales associated with the ballistic electron motion and the mean free paths associated with scattering of electrons with lattice vibrations at elevated and ambient temperatures. This is mainly due to the limitation of the purely time-resolved pump−probe measurements that typically lack the spatial resolution required to directly monitor these nonequilibrium electron dynamics. Moreover, first-principles calculations of electron−phonon coupling have not considered scenarios with elevated electron temperatures that typically occur in the first couple of picoseconds immediately after ultrafast laser excitations of metals.

In this work, we use novel ultrafast microscopy with high spatiotemporal resolution to directly measure the electron ballistic and diffusive mean free paths in gold. We find that the ballistic length of electrons following femtosecond laser irradiation is in excess of ~150 nm, which is 50% larger than the previously accepted value of 100 nm from time-of-flight measurements,[22,29,31] a value that has been accepted for over three decades. We also find that the mean free paths of electrons with Fermi−Dirac distributions are in the 20−50 nm range depending on the electronic temperature following the thermalization of the hot electron gas through carrier−carrier scattering. Density functional perturbation theory (DFPT), where we include the effects of electronic excitation with the Fermi−Dirac distribution, reveals that the electron−phonon coupling parameter is reduced at these elevated electron temperatures due to lattice hardening resulting from interband excitation. Furthermore, our DFPT calculations also

show that the mean free path of the electron gas is increased due to the reduced electron−phonon coupling at elevated electron temperatures, supporting our experimental findings.

Our direct imaging of carrier motion in thin gold films is accomplished using a home-built ultrafast super-resolution thermoreflectance microscopy capable of exciting a sample in one location and monitoring the transport of photoexcited carriers at a different location with diffraction limited lateral resolution (as schematically shown in Figure 1a). This configuration allows for the direct visualization of the spatially separated pump−probe images for a range of delay times between the two beams; details of the experimental setup are given in the Supporting Information. A characteristic spatiotemporal tracking of electron and phonon dynamics conducted for a 200 nm thick Au film through our super-resolution thermoreflectance is shown in Figure 1b. The Gaussian profile obtained from the spatial mapping at various pump−probe delay times can provide insights into the dynamics of the energy carriers in the thin film. For example, the initial (<600 fs) time regime is associated with ballistic motion of electrons away from the excited spot,[29,30,41] where the electrons still have not achieved a Fermi−Dirac distribution. In fact, through electron photoemission measurements on 30 nm gold film, Fann et al. have shown that a Fermi−Dirac distribution can only be achieved after pump−probe delays of ~670 fs,[30,41] thus providing evidence of the ballistic nature of the nonthermal electrons at these time frames. A spatial comparison between our laser spot size and the acquired probe signal during this period can provide an indication of the ballistic length of electrons following laser excitation (Figure 1c). We find that the "excess" signal relative to the laser spot, where the Gaussian intensity has decayed by

$1/e^2$, suggests that the ballistic length of electrons in gold is (on the order of ~200 nm) much larger than the previously reported value of 100 nm. Note, while we cannot systematically show differences in the ballistic mean free paths of electrons at earlier delay times due to the ~200 fs time resolution in our experiments and the ultrafast nature of the ballistic electrons traversing with velocities close to the Fermi velocity, we find that the excess signal is consistent across the nonthermal time frames of <600 fs (see Figure S8).

The ballistic length of electrons in gold has been indirectly measured via pump–probe methods through time-of-flight experiments in prior works, where the pump is incident on the front surfaces of gold films with varying thicknesses while the probe monitors the change in reflectivity of the back surface.[22,29] In so doing, the profile of the probe signal as a function of pump–probe delay time changes as a result of the variation in the traversal time of the electrons to cross the film. A variation in the profiles between 100 and 200 nm thick films has been inferred to suggest that ballistic electrons dominate the 100 nm thick film, while for the 200 nm film, diffusive transport was the dominant mechanism controlling the reflected temporal profile of the probe beam. Our results, however, suggest that the ballistic length of electrons in gold can exceed the 100 nm length scale reported in prior literature.

To support our measurements, we perform additional measurements on gold films with a very thin (~2 nm) Ti layer in-between the gold film and the substrate. As Ti has an order of magnitude higher electron–phonon coupling factor, the ballistic electrons from the laser-heated gold surface traverse the thickness of the films and scatter at the Ti layer. Due to the relatively larger time constant related with the flow of heat to the substrate through phonon–phonon coupling, heat deposited with the phonons in the Ti layer is transferred to the relatively colder Au lattice.[42] This manifests as an increase in the reflectivity of the gold surface (and a rerise in the thermoreflectance signal) on time scales of ~5 to 50 ps. This is visualized in Figure 1d for a 150 nm Au/Ti structure taken with $1/e^2$ pump and probe sizes of ~5 μm to ensure that the transport is predominantly in the through-plane direction. If the ballistic electrons are not able to reach the Ti layer, we do not expect a "rerise" in the acquired probe signal. As shown in Figure 1e (and visualized in the contour plots in Figure S4 of the Supporting Information), we observe the "rerise" in the signal even for our 173 nm thick gold film, suggesting that the ballistic length of electrons in gold is at least ~150 nm.

Next, we consider the diffusion of electrons that is mainly limited by electron–phonon scattering in gold by extracting the full-width at half-maximum (fwhm) from the Gaussian profiles at the various pump–probe delay times following electron thermalization. The slope of the square of fwhm plotted as a function of time (as shown in Figure 2a) is proportional to the thermal diffusivity (see Supporting Information). From Figure 2a, we observe two diffusion regimes, an initial fast diffusion regime for the first couple of picoseconds and a slower regime for the longer time scale. The fast diffusion coefficient obtained is D_{fast} = 94 cm^2 s^{-1}, while the slow diffusion coefficient obtained is around D_{slow} = 1.3 cm^2 s^{-1}. For the slow diffusion regime, where the electrons and phonons are in equilibrium, we can approximate the thermal diffusivity as $D = (\kappa_e + \kappa_p)/(C_e + C_p)$, where κ_e and κ_p are the electron and phonon thermal conductivities, respectively. Likewise, C_e and C_p are the electron and phonon heat capacities, respectively. Since the heat capacity of electrons and
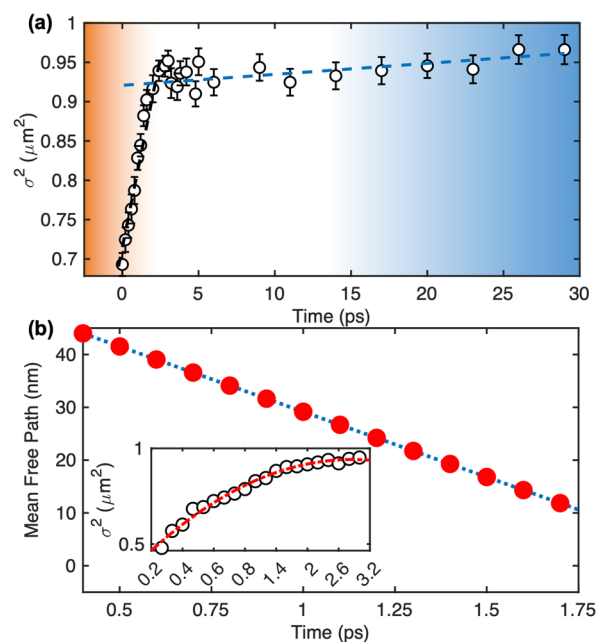

Figure 2. (a) Square of the full-width at half-maximum (σ^2) calculated from the surface response of a 200 nm thick gold film to a femtosecond pump laser at various pump–probe time delays. The slope of the σ^2 versus time is related to the thermal diffusivity. (b) Experimental mean free paths obtained from the initial fast diffusion regime (inset) where the electrons have not fully thermalized with the lattice vibrations. For time scales where the electrons achieve a Fermi–Dirac distribution and reach their peak temperature, we predict a mean free path of ~45 nm, which monotonically decreases as electron–phonon coupling progresses and the electronic subsystem losses its energy to the lattice vibrations.

the phonon thermal conductivity in gold are negligible compared to the phonon heat capacity and electron thermal conductivity, respectively, we estimate a value of $\kappa_e \approx 315 \pm 40$ W m^{-1} K^{-1}, which is in good agreement with our electrical resistivity measurements and prior literature values.[43]

For the fast diffusion regime (Figure 2a), when the electrons are predominantly out of equilibrium with the lattice, the diffusivity can be approximated by the relation $D = \kappa_e/C_e$, from which we can estimate the diffusive mean free path of electrons as shown in Figure 2b. The mean free path monotonically decreases from an initial value of ~45 to 20 nm in the first picosecond, signifying that at elevated electron temperatures, electrons can traverse longer distances in gold; initially, the electronic subsystem is at an elevated temperature, which gradually relaxes with the lattice and cools to lower temperatures in the first couple of picoseconds as predicted from a two-temperature model (see Supporting Information). Therefore, we note that the mean free paths extracted through this procedure are more reliable for time regimes before the majority of the conduction electrons have coupled to the lattice (which is approximately <1 ps after the electrons reach their peak temperature).

To support these measurements and gain spectral insights into the diffusive electron–phonon scattering processes, we perform DFPT calculations by considering both an excited electron gas where we set $k_B T_e$ as 3.1 eV (to mimmic our experiments) and when the electronic and phononic subsystems are in thermal equilibrium. The calculations of the electron–phonon coupling matrix and the mass enhance-

ment parameter that describes the strength of the coupling are carried out in dense electron and phonon wavevector grids (the details of which are given in the Supporting Information). The effect of interband electron excitation on the electronic structure is shown in Figure 3a, where a significant shift to
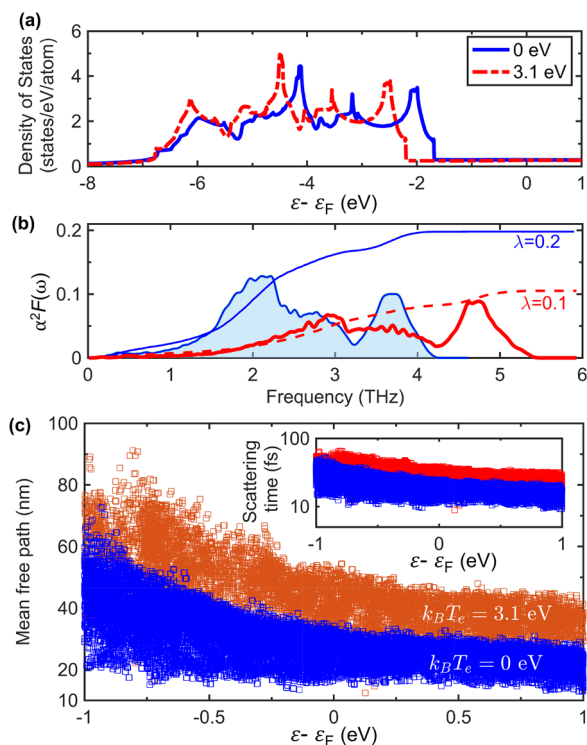

Figure 3. (a) Electronic structure calculations of electronic density of states for Au with $k_B T_e$ set to 0 and 3.1 eV. Interband excitation leads to a shift to lower energies of the d band electrons. (b) The reduced screening from the excitation also leads to phonon hardening and a shift to higher frequencies of the electron–phonon spectral function. An overall reduction of ~50% is observed for our calculated mass enhancement parameter (λ) showing the effect of interband transitions on the electron–phonon coupling in gold. (c) From the scattering times calculated for electrons (that are limited by electron–phonon interactions) in gold (inset), we predict an increase in the mean free paths of electrons at $k_B T_e$= 3.1 eV as compared to the unperturbed case, supporting our experimental findings.

lower frequencies is observed for the d bands. Moreover, due to the excitation of the $5d$ electrons, the reduced effective screening leads to an increase in the ion–ion potential, consistent with prior first-principles calculations in ref 44. The resulting lattice hardening shifts the lattice vibrations to higher frequencies as shown by the electron–phonon spectral function or the Eliashberg function, $\alpha^2 F(\omega)$, in Figure 3b. The corresponding mass enhancement parameters are also shown in the figure for comparison. This pressure increase due to the $5d$ band excitation to the higher s band results in a drastic (~50%) reduction in the electron–phonon coupling as quantified by the decrease in the mass enhancement parameter (Figure 3b). Prior calculations of the volumetric electron–phonon coupling factor have utilized a constant mass enhancement parameter for the calculations at high electron temperatures.[45−47] However, our results show that for cases when the electronic states are excited from low lying bands (for example, due to laser excitation), changes in the lattice dynamics and the spectral coupling between electrons and

phonons need to be accounted for to accurately predict the volumetric coupling between the two states.

From our *ab initio* calculation of the electron scattering times and velocities, we calculate the mean free paths of electrons for the two cases considered in this work as shown in Figure 3c. For the case with $k_B T_e$ = 3.1 eV, we predict a mean free path of ~35−53 nm for electrons near the Fermi energy, in excellent agreement with our measurement of ~45 nm, which we obtain for hot electrons when they reach the maximum temperature immediately after they acquire a Fermi−Dirac distribution (at ~600 fs). The slight discrepancies might arise from the fact that in our experiments, both electron−electron and electron−phonon scattering limit the mean free path of electrons,[36,47,48] while we have only considered scattering between the electrons and lattice vibrations in our first-principles calculations. However, the similarity in our first-principles calculations and our experimental measurement suggests that electron−electron scattering has a negligible influence on the mean free path of electrons near the Fermi energy after the electrons have achieved a Fermi−Dirac distribution in our experiments.

In summary, we have directly measured the ballistic and diffusive mean free paths of electrons in gold via our ultrafast super-resolution thermoreflectance experiments. More specifically, we show that the ballistic length of electrons in gold can exceed length scales of ~150 nm, which is far greater than the previously accepted value of 100 nm. The diffusive mean free path of electrons can reach up to ~45 nm following laser excitation of d band electrons to higher states, which is greater than the average mean free path of 35 nm predicted from first-principles calculations for an unperturbed electron gas interacting with the gold lattice. Our parameter-free *ab initio* calculations based on solving the Fermi's golden rule reveal that the increased mean free path of electrons is a direct consequence of drastic reduction in electron−phonon coupling when considering interband excitation. Our results provide important insights into understanding of hot carrier generation and transport in bulk and nanostructured noble metals, the comprehensive knowledge of which is significant for a plethora of applications such as in plasmonic devices.

■ ASSOCIATED CONTENT

Ⓢ Supporting Information

The Supporting Information is available free of charge at https://pubs.acs.org/doi/10.1021/acs.nanolett.2c03781.

Details of the experimental setup and knife-edge measurements, two-temperature model and density functional perturbation theory calculations (PDF)

■ AUTHOR INFORMATION

Corresponding Author

Ashutosh Giri − *Department of Mechanical, Industrial and Systems Engineering, University of Rhode Island, Kingston, Rhode Island 02881, United States;* ⓞ orcid.org/0000-0002-8899-4964; Email: ashgiri@uri.edu

Authors

Pravin Karna − *Department of Mechanical, Industrial and Systems Engineering, University of Rhode Island, Kingston, Rhode Island 02881, United States*

Md Shafkat Bin Hoque − *Department of Mechanical and Aerospace Engineering, University of Virginia, Charlottesville, Virginia 22904, United States*

Sandip Thakur − *Department of Mechanical, Industrial and Systems Engineering, University of Rhode Island, Kingston, Rhode Island 02881, United States;* ◉ orcid.org/0000-0002-3763-3659

Patrick E. Hopkins − *Department of Mechanical and Aerospace Engineering, University of Virginia, Charlottesville, Virginia 22904, United States; Department of Materials Science and Engineering and Department of Physics, University of Virginia, Charlottesville, Virginia 22904, United States;* ◉ orcid.org/0000-0002-3403-743X

Complete contact information is available at:
https://pubs.acs.org/10.1021/acs.nanolett.2c03781

Notes

The authors declare no competing financial interest.

■ REFERENCES

(1) Drude, P. Zur elektronentheorie der metalle; II. Teil. galvanomagnetische und thermomagnetische effecte. *Annalen der physik* **1900**, *308* (11), 369−402.

(2) Ziman, J. *Electrons and Phonons: The Theory of Transport Phenomena in Solids*; Oxford University Press: Oxford, 2001.

(3) Kittel, C. *Introduction to solid state physics*, 6th ed.; Wiley: New York, 1986.

(4) Ivanov, D. S.; Zhigilei, L. V. Combined atomistic-continuum modeling of short-pulse laser melting and disintegration of metal films. *Phys. Rev. B* **2003**, *68* (6), 064114.

(5) Ivanov, D. S.; Zhigilei, L. V. Kinetic limit of heterogeneous melting in metals. *Phys. rev. Lett.* **2007**, *98* (19), 195701.

(6) Wu, C.; Zhigilei, L. V. Nanocrystalline and polyicosahedral structure of a nanospike generated on metal surface irradiated by a single femtosecond laser pulse. *J. Phys. Chem. C* **2016**, *120* (8), 4438−4447.

(7) Brown, A. M.; Sundararaman, R.; Narang, P.; Schwartzberg, A. M.; Goddard, W. A., III; Atwater, H. A. Experimental and ab initio ultrafast carrier dynamics in plasmonic nanoparticles. *Phys. Rev. Lett.* **2017**, *118* (8), 087401.

(8) Atwater, H. A.; Polman, A. Plasmonics for improved photovoltaic devices. *Nat. mater.* **2010**, *9* (3), 205−213.

(9) Tagliabue, G.; DuChene, J. S.; Abdellah, M.; Habib, A.; Gosztola, D. J.; Hattori, Y.; Cheng, W.-H.; Zheng, K.; Canton, S. E.; Sundararaman, R.; et al. Ultrafast hot-hole injection modifies hot-electron dynamics in Au/p-GaN heterostructures. *Nat. Mater.* **2020**, *19* (12), 1312−1318.

(10) Wu, X.; Chen, G. Y.; Owens, G.; Chu, D.; Xu, H. Photothermal materials: A key platform enabling highly efficient water evaporation driven by solar energy. *Mater. Today Energy* **2019**, *12*, 277−296.

(11) Clavero, C. Plasmon-induced hot-electron generation at nanoparticle/metal-oxide interfaces for photovoltaic and photocatalytic devices. *Nat. Photon* **2014**, *8* (2), 95−103.

(12) Zheng, B. Y.; Zhao, H.; Manjavacas, A.; McClain, M.; Nordlander, P.; Halas, N. J. Distinguishing between plasmon-induced and photoexcited carriers in a device geometry. *Nat. Commun.* **2015**, *6* (1), 7797.

(13) Hernández-Acosta, M. A.; Torres-Torres, C.; Bornacelli, J.; García-Merino, J. A.; Can-Uc, B.; Rangel-Rojo, R.; Oliver, A. A comprehensive study of the nonlinear optical response exhibited by ion-implanted silica plates with Au and Pt nanostructures. *Results in Opt.* **2021**, *4* (8), 100098.

(14) Moskovits, M. The case for plasmon-derived hot carrier devices. *Nat. Nanotechnol.* **2015**, *10* (1), 6−8.

(15) Mukherjee, S.; Libisch, F.; Large, N.; Neumann, O.; Brown, L. V.; Cheng, J.; Lassiter, J. B.; Carter, E. A.; Nordlander, P.; Halas, N. J. Hot electrons do the impossible: plasmon-induced dissociation of H2 on Au. *Nano Lett.* **2013**, *13* (1), 240−247.

(16) Kale, M. J.; Avanesian, T.; Christopher, P. Direct photocatalysis by plasmonic nanostructures. *ACS Catal.* **2014**, *4* (1), 116−128.

(17) Tomko, J. A.; Runnerstrom, E. L.; Wang, Y.-S.; Chu, W.; Nolen, J. R.; Olson, D. H.; Kelley, K. P.; Cleri, A.; Nordlander, J.; Caldwell, J. D.; et al. Long-lived modulation of plasmonic absorption by ballistic thermal injection. *Nat. Nanotechnol.* **2021**, *16* (1), 47−51.

(18) Sinova, J. Thinks globally but acts locally. *Nat. Mater.* **2010**, *9* (11), 880−881.

(19) Bauer, G. E.; Saitoh, E.; Van Wees, B. J. Spin caloritronics. *Nat. Mater.* **2012**, *11* (5), 391−399.

(20) Allen, P. B. Theory of thermal relaxation of electrons in metals. *Phys. Rev. Lett.* **1987**, *59* (13), 1460−1463.

(21) Grimvall, G. *The electron-phonon interaction in metals*; North-Holland: New York, 1981.

(22) Brorson, S.; Fujimoto, J.; Ippen, E. Femtosecond electronic heat-transport dynamics in thin gold films. *Phys. Rev. Lett.* **1987**, *59* (17), 1962.

(23) Brorson, S.; Kazeroonian, A.; Moodera, J.; Face, D.; Cheng, T.; Ippen, E.; Dresselhaus, M.; Dresselhaus, G. Femtosecond room-temperature measurement of the electron-phonon coupling constant γ in metallic superconductors. *Phys. Rev. Lett.* **1990**, *64* (18), 2172.

(24) Eesley, G. Generation of nonequilibrium electron and lattice temperatures in copper by picosecond laser pulses. *Phys. Rev. B* **1986**, *33* (4), 2144.

(25) Schoenlein, R.; Lin, W.; Fujimoto, J.; Eesley, G. Femtosecond studies of nonequilibrium electronic processes in metals. *Phys. Rev. Lett.* **1987**, *58* (16), 1680.

(26) Eesley, G. Observation of nonequilibrium electron heating in copper. *Phys. Rev. Lett.* **1983**, *51* (23), 2140.

(27) Groeneveld, R. H.; Sprik, R.; Lagendijk, A. Ultrafast relaxation of electrons probed by surface plasmons at a thin silver film. *Phys. Rev. Lett.* **1990**, *64* (7), 784.

(28) Suárez, C.; Bron, W.; Juhasz, T. Dynamics and transport of electronic carriers in thin gold films. *Phys. Rev. Lett.* **1995**, *75* (24), 4536.

(29) Juhasz, T.; Elsayed-Ali, H.; Smith, G.; Suarez, C.; Bron, W. Direct measurements of the transport of nonequilibrium electrons in gold films with different crystal structures. *Phys. Rev. B* **1993**, *48* (20), 15488.

(30) Fann, W.; Storz, R.; Tom, H.; Bokor, J. Direct measurement of nonequilibrium electron-energy distributions in subpicosecond laser-heated gold films. *Phys. Rev. Lett.* **1992**, *68* (18), 2834.

(31) Hohlfeld, J.; Wellershoff, S.-S.; Güdde, J.; Conrad, U.; Jähnke, V.; Matthias, E. Electron and lattice dynamics following optical excitation of metals. *Chem. Phys.* **2000**, *251* (1-3), 237−258.

(32) Guo, L.; Xu, X. Ultrafast spectroscopy of electron-phonon coupling in gold. *J. Heat Trans.* **2014**, *136* (12), 122401.

(33) Chowdhury, I. H.; Xu, X. Heat transfer in femtosecond laser processing of metal. *Numer. Heat Transfer; A: Appl.* **2003**, *44* (3), 219−232.

(34) Kaganov, M.; Lifshitz, E.; Tanatarov, L. Relaxation between electrons and the crystalline lattice. *Soviet Physics-JETP* **1957**, *4* (2), 173−178.

(35) Anisimov, S. I.; Rethfeld, B. Theory of ultrashort laser pulse interaction with a metal. *Nonresonant Laser-Matter Interaction (NLMI-9)* **1997**, 192−203.

(36) Giri, A.; Gaskins, J. T.; Foley, B. M.; Cheaito, R.; Hopkins, P. E. Experimental evidence of excited electron number density and

temperature effects on electron-phonon coupling in gold films. *J. Appl. Phys.* **2015**, *117* (4), 044305.

(37) Groeneveld, R. H.; Sprik, R.; Lagendijk, A. Femtosecond spectroscopy of electron-electron and electron-phonon energy relaxation in Ag and Au. *Phys. Rev. B* **1995**, *51* (17), 11433.

(38) Elsayed-Ali, H.; Juhasz, T.; Smith, G.; Bron, W. Femtosecond thermoreflectivity and thermotransmissivity of polycrystalline and single-crystalline gold films. *Phys. Rev. B* **1991**, *43* (5), 4488.

(39) Brown, A. M.; Sundararaman, R.; Narang, P.; Goddard, W. A., III; Atwater, H. A. Ab initio phonon coupling and optical response of hot electrons in plasmonic metals. *Phys. Rev. B* **2016**, *94* (7), 075120.

(40) Bernardi, M.; Mustafa, J.; Neaton, J. B.; Louie, S. G. Theory and computation of hot carriers generated by surface plasmon polaritons in noble metals. *Nat. Commun.* **2015**, *6* (1), 7044.

(41) Fann, W.; Storz, R.; Tom, H.; Bokor, J. Electron thermalization in gold. *Phys. Rev. B* **1992**, *46* (20), 13592.

(42) Giri, A.; Gaskins, J. T.; Donovan, B. F.; Szwejkowski, C.; Warzoha, R. J.; Rodriguez, M. A.; Ihlefeld, J.; Hopkins, P. E. Mechanisms of nonequilibrium electron-phonon coupling and thermal conductance at interfaces. *J. Appl. Phys.* **2015**, *117* (10), 105105.

(43) Cook, J.; Meer, M. v. d. The thermal conductivity and electrical resistivity of gold from 80 to 340 K. *Can. J. Phys.* **1970**, *48* (3), 254−263.

(44) Recoules, V.; Clérouin, J.; Zérah, G.; Anglade, P.; Mazevet, S. Effect of intense laser irradiation on the lattice stability of semiconductors and metals. *Phys. Rev. Lett.* **2006**, *96* (5), 055503.

(45) Lin, Z.; Zhigilei, L. V.; Celli, V. Electron-phonon coupling and electron heat capacity of metals under conditions of strong electron-phonon nonequilibrium. *Phys. Rev. B* **2008**, *77* (7), 075133.

(46) Brown, A. M.; Sundararaman, R.; Narang, P.; Goddard, W. A., III; Atwater, H. A. Nonradiative plasmon decay and hot carrier dynamics: effects of phonons, surfaces, and geometry. *ACS Nano* **2016**, *10* (1), 957−966.

(47) Giri, A.; Hopkins, P. E. Transient thermal and nonthermal electron and phonon relaxation after short-pulsed laser heating of metals. *J. Appl. Phys.* **2015**, *118* (21), 215101.

(48) Mueller, B.; Rethfeld, B. Relaxation dynamics in laser-excited metals under nonequilibrium conditions. *Phys. Rev. B* **2013**, *87* (3), 035139.